scientific reports

Check for updates

OPEN

Crossover from two-frequency pulse compounds to escaping solitons

O. Melchert[1,2]✉, S. Willms[1,2], U. Morgner[1,2,3], I. Babushkin[1,2] & A. Demircan[1,2,3]

The nonlinear interaction of copropagating optical solitons enables a large variety of intriguing bound-states of light. We here investigate the interaction dynamics of two initially superimposed fundamental solitons at distinctly different frequencies. Both pulses are located in distinct domains of anomalous dispersion, separated by an interjacent domain of normal dispersion, so that group velocity matching can be achieved despite a vast frequency gap. We demonstrate the existence of two regions with different dynamical behavior. For small velocity mismatch we observe a domain in which a single heteronuclear pulse compound is formed, which is distinct from the usual concept of soliton molecules. The binding mechanism is realized by the mutual cross phase modulation of the interacting pulses. For large velocity mismatch both pulses escape their mutual binding and move away from each other. The crossover phase between these two cases exhibits two localized states with different velocity, consisting of a strong trapping pulse and weak trapped pulse. We detail a simplified theoretical approach which accurately estimates the parameter range in which compound states are formed. This trapping-to-escape transition allows to study the limits of pulse-bonding as a fundamental phenomenon in nonlinear optics, opening up new perspectives for the all-optical manipulation of light by light.

The nonlinear Schrödinger equation (NSE) constitutes a paradigmatic model in nonlinear optics that exhibits solitons, i.e. particle-like field solutions that exist due to a balance of dispersive and nonlinear effects[1–3]. Individual NSE solitons propagate without changing their shape and collisions between two such solitons do not affect their individual properties[4]. A characteristic of NSE solitons is the hyperbolic-secant shape, i.e. sech–shape, of their field envelope. The NSE solitons defining parameters involve the fiber parameters but a free parameter, given by the soliton duration or amplitude, is retained, allowing to define the pulse characteristics. If the NSE is perturbed by higher orders of dispersion, phase-matching effects can allow for the resonant generation of radiation[5–7]. In such a case, a soliton will suffer energy loss upon propagation. Hence, for NSE-type equations with more general dispersion relations, true solitons are not implied. However, for the particular case of anomalous second-order dispersion (2OD), vanishing third-order dispersion (3OD), and *positive* fourth-order dispersion (4OD), an exact soliton solution of sech × tanh–shape exist[8]. In contrast to a NSE soliton, the properties of this "fixed-paramter" soliton solution are fully determined by the fiber parameters. Further, for the case of anomalous 2OD, vanishing 3OD, and *negative* 4OD, an exact fixed-parameter soliton solution of sech^2–shape was specified, its interaction dynamics studied, and a continuous family of solutions was shown to exist[9,10]. For a variant in which the propagation equation is governed by negative 4OD only, "pure-quartic solitons" where reported[11]. Recently, an exact sech^2–shaped fixed-parameter soliton solution for the case of anomalous 2OD, *nonvanishing* 3OD and negative 4OD was presented, its stability proven, and its conditions of existence clarified[12–15]. For this case, an exact sech × tanh–shaped "dipole-soliton" solution was derived lately[16].

Besides such single-pulse solitary wave solutions, various types of molecule-like bound states have been reported that consist of multiple pulses. This includes bound states consisting of two identical optical pulses separated by a fixed time-delay, realized through dispersion engineering for a standard NSE[17], bound solitons arising in models of coupled NSEs[18–25], bound solitons copropagating in twin-core fibers subject to higher-order dispersion[26], and dissipative optical soliton molecule generated in passively mode-locked fiber laser[27,28]. More recently, a different kind of molecule-like bound state was reported that forms a single complex, consisting of two subpulses with roughly similar amplitudes but distinctly different center frequencies[29]. Such compound states are enabled by a propagation constant that allows for group-velocity matched copropagation of pulses in

[1]Institute of Quantum Optics, Leibniz Universität Hannover, Welfengarten 1, 30167 Hannover, Germany. [2]Cluster of Excellence PhoenixD, Welfengarten 1, 30167 Hannover, Germany. [3]Hannover Centre for Optical Technologies, Nienburger Str. 17, 30167 Hannover, Germany. ✉email: melchert@iqo.uni-hannover.de

distinct domains of anomalous dispersion, separated by an interjacent domain of normal dispersion. A mutual cross-phase modulation induced attractive potential provides the binding mechanism that holds the constituent pulses together[29]. This transfers the concept of a soliton induced strong refractive index barrier for a normally dispersive wave[30], to the interaction of pulses in distinct domains of anomalous dispersion. The former process is enabled by a general wave reflection mechanism originally reported in fluid dynamics[31], in optics referred to as the push-broom effect[32], optical event horizon[33,34], or temporal reflection[35], allowing for a strong and efficient all optical control of light pulses[36,37]. This mechanism has been shown to naturally appear in the supercontinuum generation process[38–41]. The previously studied formation of molecule-like two-frequency pulse compounds constitutes a paradigmatic example of extreme states of light, also offering intriguing insights to atom-like features of a soliton, including its ability to act as a localized trapping potential with a discrete level spectrum[29]. For a higher-order nonlinear Schrödinger equation with positive 2OD and negative 4OD, similar compound states where recently also observed, and, along with the sech^2–shaped single soliton solutions of earlier studies[9,12], identified as members of a large family of generalized dispersion Kerr solitons[42]. Objects of this type have recently been observed within a mode-locked laser cavity[43]. Dual-frequency pulses with similar pulse structure have previously also been studied experimentally in passively mode-locked fiber lasers[44], and in a model for dual-channel simultaneous modelocking based on the Swift-Hohenberg equation[45]. Further, two-color soliton microcomb states where reported in theoretical studies of Kerr microresonators in terms of the Lugiato-Lefever equation (LLE) with two separate domains of anomalous dispersion[46], and in the standard LLE with added negative quartic group-velocity dispersion[47]. Bound states of distinct solitons, i.e. composite solitons, with a very similar pulse structure where reported in a combined theoretical and experimental study of the Kerr multistability in the LLE[48]. The properties of these kind of objects, which are referred to by a variety of names such as dual-frequency pulses[44], two-color soliton states[46], two-frequency soliton molecules[29], composite solitons[48], and, polychromatic soliton molecules[43], are largely unexplored. Subsequently we refer to these objects simply as pulse compounds.

Here, we study the interaction dynamics of two initially superimposed fundamental solitons at distinctly different center frequencies in terms of a propagation constant for which the group velocity dispersion (GVD) has downward parabolic symmetry. Such a profile allows to parametrically define pairs of center frequencies at which the local dispersion parameters have the same absolute values at any order. This reduces the complexity of the underlying model and allows to explore the influence of the nonlinear interaction on the model dynamics more directly. Specifically, we here investigate how an initial group-velocity (GV) mismatch affects the formation of two-frequency pulse compounds. While it was shown that such compound states can compensate sufficiently small GV mismatches through excitation of internal degrees of freedom[29], reminiscent of molecular vibrations, this puts their robustness to the test and sheds more light on the binding mechanism that holds the subpulses together. In the limit of large GV mismatch we observe a crossover from the formation of two-frequency compound states to escaping solitons. We demonstrate that the crossover region exhibits pulse compounds consisting of a strong trapping pulse and a weak trapped pulse, GV matched despite a large center frequency mismatch. Building upon the interaction of a single soliton with a localized attractive potential in terms of a perturbed NSE, we derive a simplified theoretical approach that suggests an analogy to classical mechanics and allows to accurately estimate the parameter range wherein pulse compounds are formed.

Results

We model z-propagation of the real-valued optical field $E(z,t) = \sum_\omega E_\omega(z)e^{-i\omega t}$ in a periodic t-domain of extend T with $\omega \in \frac{2\pi}{T}\mathbb{Z}$ in terms of the complex-valued analytic signal $\mathcal{E}(z,t) = 2\sum_{\omega>0} E_\omega(z)e^{-i\omega t}$ via the first-order nonlinear propagation equation

$$i\partial_z \mathcal{E}_\omega + \beta(\omega)\mathcal{E}_\omega + \gamma(\omega)\left(|\mathcal{E}|^2\mathcal{E}\right)_{\omega>0} = 0, \tag{1}$$

describing single mode propagation in a nonlinear waveguide[49,50]. In Eq. (1), $\beta(\omega)$ denotes the propagation constant and $\gamma(\omega)$ specifies a coefficient function for its nonlinear part. The characteristics of both are illustrated in Fig. 1. Considering the reference frequency $\omega_0 = 2$ rad/fs, the propagation constant is modeled by the polynomial expression

$$\beta(\omega) = \sum_{n=0}^{4} \frac{\beta_n}{n!}(\omega-\omega_0)^n, \tag{2}$$

with $\beta_0 = 25.0\,\mu\mathrm{m}^{-1}$, $\beta_1 = 13.0\,\mathrm{fs}\,\mu\mathrm{m}^{-1}$, $\beta_2 = 0.1\,\mathrm{fs}^2\,\mu\mathrm{m}^{-1}$, $\beta_3 = 0.0\,\mathrm{fs}^3\,\mu\mathrm{m}^{-1}$, and $\beta_4 = -0.7\,\mathrm{fs}^4\,\mu\mathrm{m}^{-1}$. For our subsequent numerical analysis we consider the transformed field $\mathcal{E}'_\omega(z) = \mathcal{E}_\omega(z)\exp(i\frac{\omega}{v_0}z)$, shifted to a moving frame of reference. The time-domain representation $\mathcal{E}'(z,t)$ then corresponds to the time-shifted analytic signal $\mathcal{E}(z,\tau = t - z/v_0)$. The reference velocity v_0 is chosen so that the time-domain dynamics appears slow. We subsequently set $v_0 \equiv v_g(\omega_0) \approx 0.0769\,\mu\mathrm{m/fs}$, wherein $v_g(\omega) \equiv [\partial_\omega\beta(\omega)]^{-1}$ signifies the group-velocity, see Fig. 1a. As can be seen in Fig. 1b, the group velocity dispersion (GVD) $\beta_2(\omega) = \partial^2_\omega\beta(\omega)$ assumes a downward parabolic shape, which, in terms of the angular frequency detuning $\Omega = \omega - \omega_0$, can be expressed as $\beta_2(\omega_0+\Omega) = \beta_2 + \frac{\beta_4}{2}\Omega^2$. It is thus similar to the setup considered in reference[42] in which a NSE subject to positive quadratic and additional negative quartic dispersion was studied (see "Methods" for details). It is further a simplified variant of the propagation constant with a non-symmetric GVD, for which we previously studied the interaction of solitons leading to the formation of heteronuclear soliton molecules[29]. Here, the zero-dispersion detunings are given by the roots of the GVD at $\Omega_{\mathrm{ZDW1,ZDW2}} = \pm\sqrt{-2\beta_2/\beta_4} \approx \pm 0.535$ rad/fs, specifying two zero-dispersion frequencies at $(\omega_{\mathrm{ZDW1}}, \omega_{\mathrm{ZDW2}}) \approx (1.465, 2.535)$ rad/fs. The coefficient function of the nonlinearity is modeled as

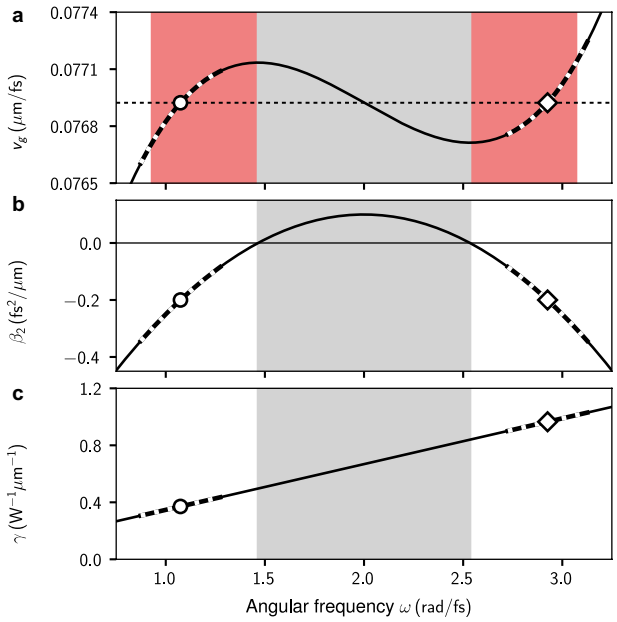

Figure 1. Specifics of the considered z-propagation model. (**a**) Frequency dependence of the group velocity. Frequency ranges shaded in red allow for group-velocity matched co-propagation of light pulses in separate regions of anomalous dispersion. Horizontal dashed line indicates reference velocity v_0. (**b**) Group velocity dispersion profile. (**c**) Nonlinear coefficient function. In all subplots, normally dispersive frequency ranges are shaded gray. Open circle and open square indicate the loci of ω_{GVM1} and ω_{GVM2}, respectively. Thicker dashed parts of curves indicate the angular frequency ranges covered by the parameter sweep. Polynomial models for $\beta(\omega)$ and $\gamma(\omega)$ are detailed in the main text.

$$\gamma(\omega) = \gamma_0 + \gamma_1\omega, \tag{3}$$

with $\gamma_0 = 0.026\,\mathrm{W^{-1}\mu m^{-1}}$ and $\gamma_1 = 0.321\,\mathrm{fs\,W^{-1}\mu m^{-1}}$, see Fig. 1c. To better understand the time-frequency interrelations of the analytic signal at a selected propagation distance z, we consider its spectrogram[51]

$$P_S(\tau,\omega) = \frac{1}{2\pi}\left|\int \mathcal{E}(z,\tau')h(\tau'-\tau)e^{-i\omega\tau}\,\mathrm{d}\tau'\right|^2, \tag{4}$$

wherein $h(x) = \exp(-x^2/2\sigma^2)$ specifies a Gaussian window function with root-mean-square width σ, used to localize $\mathcal{E}(z,\tau)$ in time.

Equation (1) is free from the slowly varying envelope approximation but can be reduced to the generalized nonlinear Schrödinger equation by introduction of a complex envelope for a suitable center frequency[49]. By assuming $\gamma = \mathrm{const.}$, it can further be reduced to a standard NSE with higher orders of dispersion. For the propagation of an initial field in terms of Eq. (1) we use a pseudospectral scheme implementing z-propagation using a fourth-order Runge-Kutta method[52].

Initial conditions. As pointed out above, the GVD is symmetric about $\omega_0 = 2\,\mathrm{rad/fs}$. Two frequencies are group-velocity (GV) matched to ω_0. In terms of the angular frequency detuning they are located at $\Omega_{\mathrm{GVM1,GVM2}} = \pm\sqrt{-6\beta_2/\beta_4} \approx \pm 0.926\,\mathrm{rad/fs}$, specifying group-velocity matched frequencies at $(\omega_{\mathrm{GVM1}}, \omega_{\mathrm{GVM2}}) \approx (1.074, 2.926)\,\mathrm{rad/fs}$, see Fig. 1a. Both frequencies are located in distinct domains of anomalous dispersion realized by the considered propagation constant, see Fig. 1b. In general, group-velocity matched co-propagation of anomalously dispersive light pulses is possible in the frequency ranges highlighted in red in Fig. 1a. More specifically, for the considered propagation constant, a mode in range $\omega \in (0.931\,\mathrm{rad/fs},\ \omega_{\mathrm{ZDW1}})$ is GV matched to a mode in $\omega \in (\omega_{\mathrm{ZDW2}},\ 3.069\,\mathrm{rad/fs})$.

Subsequently we will consider two fundamental solitons with duration $t_0 = 20\,\mathrm{fs}$ at distinctly different center frequencies $\omega_1 = \omega_{\mathrm{GVM1}} - \Delta\omega$ and $\omega_2 = \omega_{\mathrm{GVM2}} + \Delta\omega$, with frequency offset parameter $\Delta\omega \in (-0.2, 0.2)\,\mathrm{rad/fs}$. A parameter sweep over these values of $\Delta\omega$ covers the frequency ranges highlighted by the thickened dashed curves in Fig. 1. A full initial condition for the real-valued optical field reads

$$E(0,t) = \mathrm{Re}\left[A_1\,e^{-i\omega_1 t}\mathrm{sech}(t/t_0) + A_2\,e^{-i\omega_2 t}\mathrm{sech}(t/t_0)\right]. \tag{5}$$

The initial pulses are specified by the amplitude condition for a fundamental soliton, given by $A_{1,2} = \sqrt{|\beta_2(\omega_{1,2})|/\gamma(\omega_{1,2})}/t_0$. Thus, for any considered value of $\Delta\omega$, both initial solitons will have matching dispersion lengths, i.e. $L_{D,1} = L_{D,2}$ with $L_{D,1} = t_0^2/|\beta_2(\omega_1)|$ and $L_{D,2} = t_0^2/|\beta_2(\omega_2)|$. However, since $A_1 = \sqrt{\gamma(\omega_2)/\gamma(\omega_1)}A_2$, their amplitudes satisfy $A_1 > A_2$. The group-velocity mismatch of both solitons

vanishes only at $\Delta\omega = 0$ and increases for increasing absolute values of $\Delta\omega$. For example, for $\Delta\omega < 0$ one has $v_g(\omega_1) \geq v_0 \geq v_g(\omega_2)$. In the considered frame of reference, a localized pulse with $v < v_0$ will move towards larger values of τ for increasing distance z.

The solitons injected at ω_1 and ω_2 are subject to higher orders of dispersion, which, in principle, causes their velocities to slightly deviate from their bare group-velocities $v_g(\omega_1)$ and $v_g(\omega_2)$, respectively[5,53]. For a soliton with center frequency ω_s and duration t_s, this might be taken into account by considering a "corrected" soliton velocity[54] $v_g'(\omega_s, t_s) = \left[\beta_1(\omega_s) - \beta_2(\omega_s)/(\omega_s t_s^2) + \beta_3(\omega_s)/(6t_s^2)\right]^{-1}$. For the full range of simulation parameters considered in the presented study, the largest relative difference of these velocities was found to be $|v_g - v_g'|/v_g < 10^{-4}$. Subsequently we opted to use the usual group-velocity v_g when referring to the velocity of the initial solitons.

Propagation dynamics of limiting cases. Our earlier study of the interaction dynamics of initially overlapping group-velocity matched fundamental solitons with a vast frequency gap[29], suggests that in the limiting case of group-velocity matched initial solitons [$\Delta\omega = 0$ rad/fs], a heteronuclear two-frequency pulse compound will form. The evolution of a corresponding initial condition in the propagation range $z = 0{-}25$ mm is shown in Fig. 2a. The composite pulse generated by this initial condition, highlighted in the spectrogram in Fig. 2b, consists of two subpulses with roughly similar amplitudes but distinctly different center frequencies. From the spectral intensity $|\mathcal{E}_\omega|^2$ and the spectrogram P_S, the vast frequency gap between both subpulses is clearly evident. It generates resonant radiation upon propagation and leads to a kind of "radiating" compound state. In Fig. 2b, these resonances are signaled by trains of nodes that separate from the localized state. A thorough analysis of a pulse compound with a similar composition was detailed in reference[29] [see Fig. 2(f) of that reference]. The binding mechanism that leads to the formation of such a composite pulse is realized by the mutual cross-phase modulation between its interacting subpulses[29]. The resulting pulse compounds are quite robust: small initial group-velocity mismatches can be compensated by frequency shifts of the subpulse center frequencies. This enables intriguing internal dynamics, reminiscent of molecular vibrations, examined more closely in Fig. 4 below. In the limiting case of a large group-velocity mismatch of the initial solitons, i.e. for large absolute values of $\Delta\omega$, we expect that both pulses escape their mutual binding. This is demonstrated for $\Delta\omega = -0.17$ rad/fs in Fig. 2e,f. As evident from the time-domain propagation dynamics in Fig. 2e, two separate localized states with nonzero relative velocity can indeed be identified. They can be distinguished well in the spectrogram in Fig. 2f, indicating no notable trapping by either pulse.

A crossover from the formation of two-frequency soliton compounds to escaping solitons can be expected based on two arguments. First, consider the point of view of mutual trapping of each pulse by a cross-phase modulation induced attractive potential formed by the other pulse[29]. Then, a classical mechanics interpretation of the propagation scenario suggests the existence of an escape velocity, sufficient for a particle to escape its trapping potential. We explore this analogy in more detail below. Second, for offset frequencies $\Delta\omega > 0.143$ rad/fs, i.e. $\omega_1 < 0.931$ rad/fs and $\omega_2 > 2.926$ rad/fs, no mode can be group-velocity matched to either initial soliton, see Fig. 1a. Having demonstrated the propagation dynamics for two specific values of the frequency offset parameter $\Delta\omega$, a thorough investigation of the crossover between the above limiting-cases in terms of $\Delta\omega$ is in order.

Crossover from mutual trapping to escape. To better characterize the crossover from mutual trapping to unhindered escape of the initial solitons, we track the velocities of the dominant localized pulses in each domain of anomalous dispersion. In Fig. 3b, the asymptotic velocities associated with the initial solitons at ω_1 and ω_2 are labeled v_1 and v_2, respectively. In relation to the two limiting cases illustrated earlier, we find that at $\Delta\omega = 0$ rad/fs (cf. Fig. 2a) the velocities of the compounds subpulses match each other and are in good agreement with the group-velocities of the initial solitons. At $\Delta\omega = -0.17$ rad/fs (cf. Fig. 2e) we find that the dominant pulses in each region of anomalous dispersion are clearly distinct, again in agreement with the group-velocities of the initial solitons. In between, a sudden crossover occurs at $\Delta\omega_c^{(-)} \approx -0.075$ rad/fs, where v_2 shifts from $v_2 = v_1 \lesssim v_g(\omega_1)$ [for $\Delta\omega_c^{(-)} < \Delta\omega < 0$] to $v_2 = v_g(\omega_2)$ [for $\Delta\omega < \Delta\omega_c^{(-)}$], see Fig. 3b.

Matching subpulse velocities in the range $\Delta\omega_c^{(-)} < \Delta\omega < 0$ result from an initial transient propagation regime during which the mutual interaction of the initially superimposed pulses causes both pulse center frequencies to shift, thereby also changing the pulse spectrum. In this parameter range we observe that the soliton with higher amplitude, i.e. the soliton initially at ω_1, assumes a dominant role. While the effect on this pulse is small, the effect on the pulse initially at ω_2 is rather large. This is shown in Fig. 4, where we detail a simulation run at $\Delta\omega = -0.05$ rad/fs. An initial transient behavior in range $z < 10$ mm is well visible, see Fig. 4a,b. In the latter, the initial velocity mismatch of both pulses induces a vivid dynamics. This is demonstrated in Fig. 4e, where the internal dynamics of the composite pulse in terms of the separation and relative-velocity of its subpulses, reminiscent of molecular vibrations, is shown. For this example we find the asymptotic frequency shifts $\omega_1 = 1.124$ rad/fs $\rightarrow \omega_1' \approx 1.113$ rad/fs (Fig. 4c) and $\omega_2 = 2.876$ rad/fs $\rightarrow \omega_2' \approx 2.949$ rad/fs (Fig. 4d). The frequency up-shift $\omega_2 \rightarrow \omega_2'$ is expected to result in a pulse velocity for which $v_g(\omega_2') > v_g(\omega_2)$ (cf. Fig. 1a). More precisely, we find the velocity shift $v_g(\omega_2) = 0.076868\,\mu$m/fs $\rightarrow v_g(\omega_2') = 0.07695\,\mu$m/fs in agreement with the data shown in Fig. 3b. As evident from Fig. 4a, radiation is emitted predominantly in the initial stage of the pulse compounds formation process.

We find that in the vicinity of $\Delta\omega_c^{(-)}$, the asymptotic state is characterized by two distinct pulse compounds. The z-evolution of a corresponding initial condition at $\Delta\omega = -0.1$ rad/fs is shown in Fig. 2c,d. Therein, the time-domain propagation dynamics (left panel of Fig. 2c) shows two localized pulses that separate from each other for increasing propagation distance. As evident from the spectrogram at $z = 25$ mm (Fig. 2d), the two localized pulses are actually pulse compounds (labeled C1 and C2 in Fig. 2d), each consisting of a strong trapping pulse and a weak trapped pulse. An analogous phenomenon, referred to as development of a "soliton shadow", "mixing",

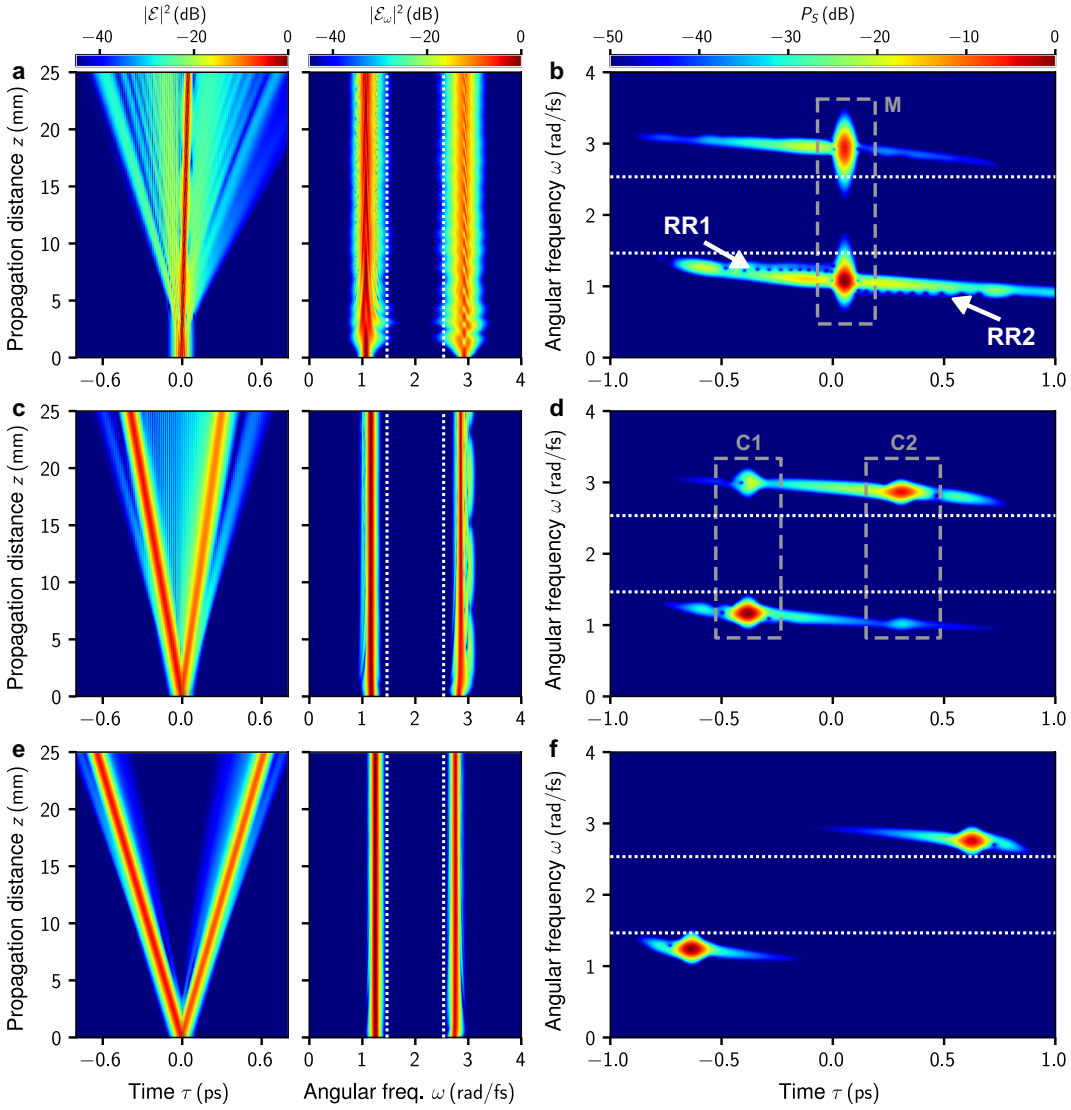

Figure 2. Exemplary propagation dynamics. (**a**) Evolution of the normalized time-domain intensity $|\mathcal{E}(z,t)|^2/\max[|\mathcal{E}(z=0\,\mathrm{mm},t)|^2]$ and normalized spectral intensity $|\mathcal{E}_\omega(z)|^2/\max[|\mathcal{E}_\omega(z=0\,\mathrm{mm})|^2]$ of the analytic signal for $\Delta\omega = 0$ rad/fs. Vertical dashed lines indicate zero dispersion points. (**b**) Analytic signal spectrogram at $z = 25$ mm for $\Delta\omega = 0$ rad/fs. Horizontal dashed lines indicate zero dispersion points. Dashed box (labeled M) encloses a molecule-like compound state. Trains of nodes signaling generation of resonant radiation are labeled RR1 and RR2. (**c**,**d**) Same as (**a**,**b**) for $\Delta\omega = -0.1$ rad/fs. In (**d**), the two dashed boxes (labeled C1 and C2) enclose pulse compounds each characterized by a strong trapping pulse and a weak trapped pulse. (**e**,**f**) same as (**a**,**b**) for $\Delta\omega = -0.18$ rad/fs. Spectrograms are computed using $\sigma = 20$ fs in Eq. (4).

or "soliton-radiation trapping", exists for coupled NSEs describing soliton propagation in birefringent fibers[21,25], and gas-filled hollow-core photonic crystal fibers[55]. One of the main differences to other works is that we here allow for group velocity matching across a vast frequency gap, which plays an important role in observing this effect. For this reason, other studies of initially superimposed solitons with center frequency mismatch did not observe such an effect[56,57]. Figure 5 shows a more comprehensive analysis of the individual pulse compounds. As evident from Fig. 5a, the time-domain intensity of both pulse compounds exhibit a fringe pattern signaling the superposition of subpulses with a significant center frequency mismatch. In Fig. 5b,c (Fig. 5d,e), the spectrum of the compound labeled C1 [C2] is put under scrutiny. In either case, both subpulses are group velocity matched and a phase-matching analysis for the strong trapping pulse indicates no generation of resonant radiation[6,7], see Fig. 5b,d. This is different from the radiating molecule in Fig. 2a.

For $\Delta\omega < \Delta\omega_c^{(-)}$, i.e. beyond the crossover region, the trapping phenomenon changes qualitatively. This can be seen from the overlap parameter

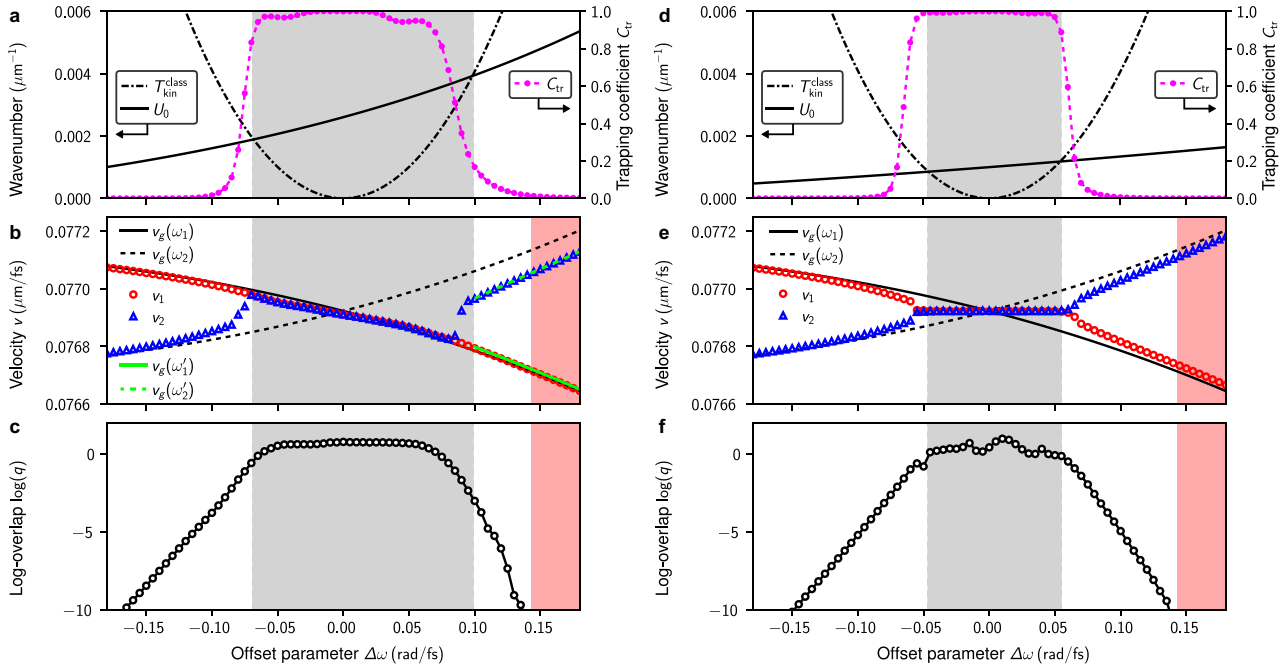

Figure 3. Characterization of the crossover from mutual trapping to escape. (**a**–**c**) Results for $\gamma(\omega)$ given by Eq. (3). (**a**) Point particle motion in an attractive potential. The particle can escape the well if its kinetic energy $T_{\mathrm{kin}}^{\mathrm{class}}$ exceeds the potential depth U_0 (see text for details). Parameter range in which the particle cannot escape the well is shaded gray. Secondary ordinate shows the trapping coefficient C_{tr} computed in a simplified model for a soliton interacting with a localized attractive potential (see text for details). (**b**) Comparison of observed asymptotic velocities v_1 and v_2 of the dominant localized pulses in the distinct domains of anomalous dispersion and corresponding propagation constant based group-velocities v_g. Light-green solid and dashed lines indicate the group velocities $v_g(\omega_1')$ and $v_g(\omega_2')$, obtained for the shifted pulse center frequencies ω_1' and ω_2', respectively (see text for details). (**c**) Logarithm of the overlap parameter q at $z = 25$ mm, quantifying the degree of mutual trapping (see text for details). Shaded area beyond $\Delta\omega \approx 0.143$ rad/fs indicates region in which group-velocity matching cannot be achieved, cf. Fig. 1a. (**d**–**f**) Same as (**a**–**c**) considering $\gamma(\omega) = \gamma_0$.

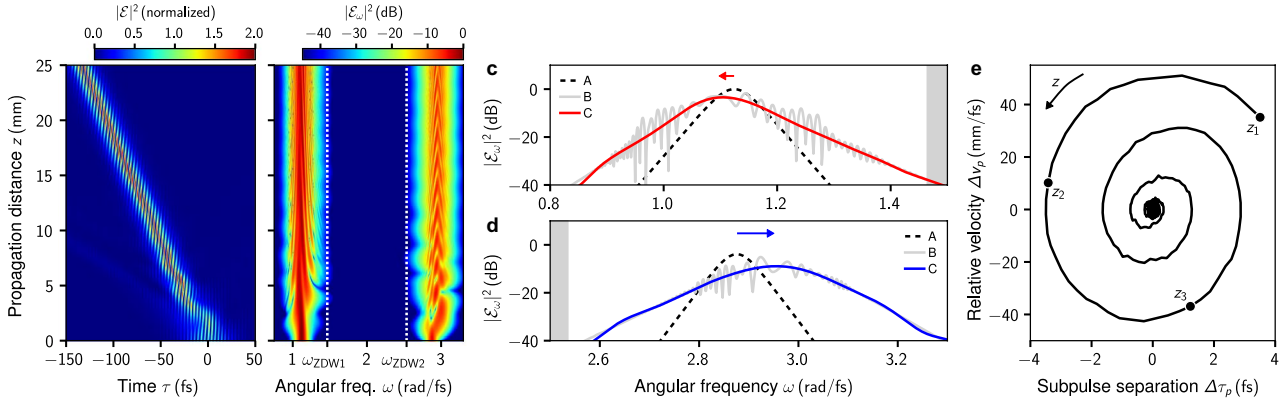

Figure 4. Formation of a two-frequency pulse compound at $\Delta\omega = -0.05$ rad/fs. Evolution of (**a**) normalized time-domain intensity $|\mathcal{E}(z,t)|^2/\max[|\mathcal{E}(z=0\,\mathrm{mm},t)|^2]$ (shown on linear scale), and (**b**) normalized spectrum $|\mathcal{E}_\omega(z)|^2/\max[|\mathcal{E}_\omega(z=0\,\mathrm{mm})|^2]$. (**c**) Spectrum in the frequency range (0.8, 1.5) rad/fs, showing the initial spectrum at $z = 0$ mm (labeled A), the full spectrum at $z = 25$ mm (labeled B), and a filtered spectrum at $z = 25$ mm (labeled C), which excludes the free radiation and highlights the subpulse in the shown frequency range. Superimposed arrow indicates direction and size of observed frequency shift (numeric values are quoted in the text). (**d**) Same as (**c**) for frequency range (2.5, 3.3) rad/fs. In (**c**,**d**) the domain of normal dispersion is shaded gray. (**e**) Internal dynamics of the pulse compound described in terms of separation (Δt_p) and relative velocity (Δv_p) of its subpulses. Trajectory in (Δt_p, Δv_p)-plane is shown for $z > 4$ mm. Markers indicate propagation distances $(z_1, z_2, z_3) = (4, 5, 6)$ mm.

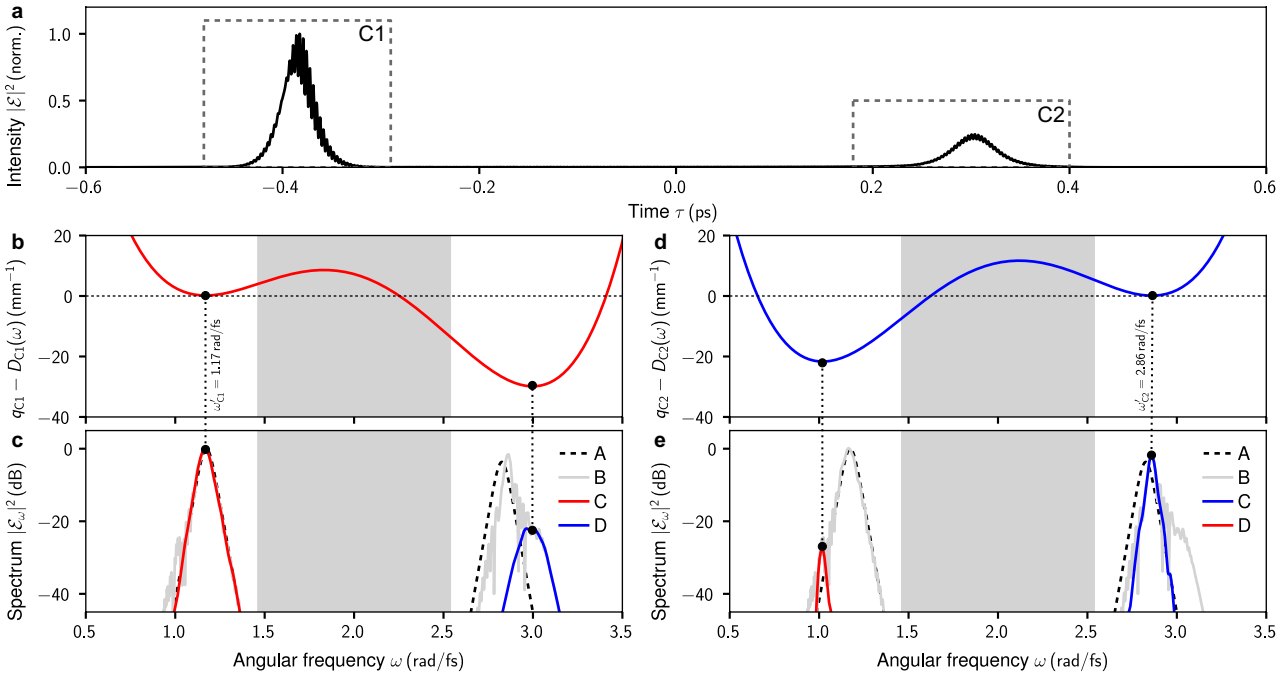

Figure 5. Detailed analysis of the pulse compounds C1 and C2 of Fig. 2d at $z = 25$ mm. (**a**) Normalized time-domain intensity $|\mathcal{E}|^2/\max[|\mathcal{E}|^2]$. (**b**) Phase matching analysis for the strong trapping pulse of C1. Shift of the soliton wavenumber $q_{C1} = \gamma(\omega'_{C1})P_0/2$ and wavenumber $D_{C1}(\omega) = \beta(\omega) - \beta(\omega'_{C1}) - \beta_1(\omega'_{C1})(\omega - \omega'_{C1})$, where P_0 is the peak intensity of the strong trapping pulse and ω'_{C1} is its center frequency. Local extrema indicate group velocity matching with the strong trapping pulse. Frequencies at which resonant radiation might be expected are indicated by the roots of $q_{C1} - D_{C1}(\omega)$. (**c**) Normalized spectrum $|\mathcal{E}_\omega(z)|^2/\max[|\mathcal{E}_\omega(z = 0\,\text{mm})|^2]$ showing the initial spectrum at $z = 0$ mm (labeled A), full spectrum at $z = 25$ mm (labeled B), and spectra of the strong trapping pulse (labeled C) and weak trapped pulse (labeled D) of C1. (**d**,**e**) Same as (**b**,**c**) for C2.

$$q(z) = \frac{\int I_1(z)I_2(z)\,\mathrm{d}\tau}{\int I_1(0)I_2(0)\,\mathrm{d}\tau}, \tag{6}$$

in which $I_1(z) = |\sum_{\omega<\omega_{ZDW1}} \mathcal{E}_\omega(z)e^{-i\omega t}|^2$ and $I_2(z) = |\sum_{\omega>\omega_{ZDW2}} \mathcal{E}_\omega(z)e^{-i\omega t}|^2$ are the time-domain intensity profiles of the pulse components restricted to separate regions of anomalous dispersion. It quantifies the degree of mutual trapping and is shown in Fig. 3c. For the limiting case of the soliton molecule ($\Delta\omega = 0$ rad/fs; Fig. 2a) we find $q \approx 2.1$ at $z = 25$ mm. In the range $\Delta\omega < \Delta\omega_c^{(-)}$, i.e. progressing towards increasingly negative values of the frequency offset parameter, it shows an exponential decrease in support of a strong-trapping to weak-trapping transition. We find this also confirmed by comparing the spectrograms in Fig. 2d,f.

A similar crossover occurs for increasing positive values of the frequency offset parameter at $\Delta\omega_c^{(+)} \approx 0.08$ rad/fs. For $\Delta\omega < \Delta\omega_c^{(+)}$ the values of v_2 and v_1 coincide and are again in well agreement with $v_g(\omega_1)$, see Fig. 3b. For $\Delta\omega < \Delta\omega_c^{(+)}$, v_2 crosses over to a value that follows the trend of $v_g(\omega_2)$, but exhibits the systematic deviation $v_g(\omega_2) - v_2 \approx 0.00007$ µm/fs. This systematic deviation is again a consequence of the perturbation imposed by the presence of a superimposed pulse in the initial condition. As pointed out earlier, the direct overlap of two solitons at $z = 0$ mm leads to an initial transient stage, during which their mutual interaction causes both pulse center frequencies to shift. Here, the effect on the pulse initially at ω_1 is again small and the effect on the pulse initially at ω_2 is rather large. Analyzing the simulation run at $\Delta\omega = 0.12$ rad/fs, we find the frequency shifts $\omega_1 = 0.954$ rad/fs $\rightarrow \omega'_1 \approx 0.961$ rad/fs and $\omega_2 = 3.046$ rad/fs $\rightarrow \omega'_2 \approx 2.991$ rad/fs. The frequency down-shift $\omega_2 \rightarrow \omega'_2$ is expected to result in a pulse velocity for which $v_g(\omega'_2) < v_g(\omega_2)$ (cf. Fig. 1a). As evident from Fig. 3b, the pulse velocities $v_g(\omega'_1)$ and $v_g(\omega'_2)$ obtained for the shifted center frequencies are in excellent agreement with the observed pulse velocities (see light-green solid and dashed lines in Fig. 3b). As pointed out above, beyond $\Delta\omega = 0.143$ rad/fs, group velocity matching is not possible (shaded region in Fig. 3). This is reflected by the overlap parameter q, dropping down to negligible values for $\Delta\omega > 0.143$ rad/fs. We observe a shift of both pulse center frequencies towards each other for $\Delta\omega > 0$, while they shift away from each other for $\Delta\omega < 0$ (see the example detailed in Figs. 4c,d). This results in group-velocity matching in the domain where pulse compounds are formed, This is different from studies of the unperturbed NSE, where the center frequencies of initially overlapping solitons where reported to shift towards each other for any reasonable initial frequency separation[58].

To clarify how the term $\propto \gamma_1\omega$ in the definition of $\gamma(\omega)$ [Eq. (3)] affects our observations, we repeated the above parameter study using the modified coefficient function $\gamma(\omega) = \gamma_0$. This setting can be reduced to a standard NSE with higher orders of dispersion (see "Methods" for details), similar to the model in which generalized dispersion Kerr solitons were studied recently[42]. Considering this simplified coefficient function, the above

parameter study involves two initial solitons with matching dispersion lengths [$L_{D,1} = L_{D,2}$] and equal amplitudes [$A_1 = A_2$]. As shown in Fig. 3e, across the region of compound state formation (i.e. for $|\Delta\omega| < 0.065$ rad/fs), the asymptotic velocities v_1 and v_2 are not longer dominated by any particular pulse. Instead, the resulting composite pulse has velocity v_0. This is, again, achieved by a shift of the pulses center frequencies during an initial transient stage. In comparison to the case where $\gamma(\omega)$ is modeled via Eq. (3), we find that the region of compound state formation is narrower. Despite the higher orders of dispersion featured by Eq. (1), the results reported in Fig. 3e are in good qualitative agreement with the interaction dynamics of initially overlapping, group-velocity mismatched solitons in a model of two nonlinearly coupled NSEs[56]. Also, a systematically smaller value of the overlap parameter q is evident in Fig. 3f. Let us comment on the characteristics of the pulse compounds in the vicinity of the crossover. The distinct features of C1 and C2 in Fig. 5 are solely due to the unsymmetry caused by the coefficient function $\gamma(\omega)$ given by Eq. (3). Considering the above modified coefficient function, we find that the spectra of C1 and C2 are simply related by symmetry, i.e. we can obtain C2 by inversion of C1 about $\omega_0 = 2$ rad/fs.

Discussion

For the whole range of frequency offsets considered in our numerical simulations, we find that the observed velocity v_1 closely follows the group velocity $v_g(\omega_1)$. Both are associated with the initial fundamental soliton with the larger amplitude. We here find that the observed velocity v_2 can match v_1 in the range -0.075 rad/fs $< \Delta\omega < 0.08$ rad/fs, specifying the range within which heteronuclear pulse compounds are formed by the considered initial conditions. Outside this range, the formation of a single two-frequency soliton molecule is inhibited, with two localized pulses separating from each other and suppressed trapping for large absolute values of the frequency offset parameter.

We found that we can estimate the domain of molecule formation in terms of a simplified theoretical approach (see "Methods" for details). In the latter, the dynamics of a two-pulse initial condition of the form of Eq. (5), governed by the nonlinear propagation equation Eq. (1), is approximated by the dynamics of a single pulse evolving under a nonlinear Schrödinger equation with localized attractive potential, given by

$$i\partial_z\phi(z,\tau') + \left[i\beta_1'\partial_{\tau'} - \frac{\beta_2'}{2}\partial_{\tau'}^2 - U(\tau') + \gamma'|\phi(z,\tau')|^2\right]\phi(z,\tau') = 0. \tag{7}$$

Therein the complex envelope $\phi(z,\tau')$ describes the dynamics of the subpulse with smaller amplitude, i.e. the subpulse at ω_2. The potential well $U(\tau')$ is related to the subpulse with higher amplitude, i.e. the subpulse at ω_1, and is given by $U(\tau') = -U_0\,\mathrm{sech}^2(\tau'/t_0)$ with potential depth

$$U_0 = 2\frac{\gamma(\omega_2)}{\gamma(\omega_1)}\frac{|\beta_2(\omega_1)|}{t_0^2}. \tag{8}$$

Further, $\beta_1' = \beta_1(\omega_2) - \beta_1(\omega_1)$, $\beta_2' = \beta_2(\omega_2)$, $\gamma' = \gamma(\omega_2)$, and $\tau' = t - \beta_1(\omega_1)z$. A similar approximation, for the special case of group-velocity matched propagation $\beta_1' = 0$, was recently used to demonstrate trapped states in a soliton-induced refractive index well[29]. Equation (7) suggests an analogy to a one-dimensional Schrödinger equation for a fictitious particle of mass $m = -1/\beta_2'$, evolving in an attractive potential localized along the τ' axis. The relative velocity between the soliton and the potential is β_1'. From a classical mechanics point of view we might expect that a particle, initially located at the potential center at $\tau' = 0$, escapes the potential well if its "classical" kinetic energy along the τ'-axis, given by

$$T_{\mathrm{kin}}^{\mathrm{class}} = \frac{m}{2}\beta_1'^2 = -\frac{[\beta_1(\omega_2) - \beta_1(\omega_1)]^2}{2\beta_2(\omega_2)}, \tag{9}$$

exceeds the potential depth U_0. In other words, for $T_{\mathrm{kin}}^{\mathrm{class}} < U_0$ we expect the particle to remain trapped by the potential. For the original model, defined by Eq. (1), this might be used to approximately estimate the domain in which compound states are formed. The results of this simplified theoretical approach are summarized in Fig. 3a,d, where $T_{\mathrm{kin}}^{\mathrm{class}}$ and U_0 are shown as function of the frequency offset parameter $\Delta\omega$. For example, considering the setup with $\gamma(\omega)$ defined by Eq. (3), the condition $T_{\mathrm{kin}}^{\mathrm{class}} < U_0$ is satisfied for -0.068 rad/fs $< \Delta\omega < 0.098$ rad/fs (Fig. 3a). Despite the various simplifying assumptions that led to the above trapping condition, the estimated bounds for the domain of compound state formation are in excellent agreement with the observed bounds discussed above. In Fig. 3a,d we complement the findings based on the classical mechanics analogy by probing the trapping-to-escape transition of a soliton in a potential well in terms of Eq. (20) via numerical simulations. We therefore computed a trapping coefficient, defined by

$$C_{\mathrm{tr}} = \frac{1}{N}\int_{-10\,t_0}^{10\,t_0} |\phi(z,\tau')|^2\,\mathrm{d}\tau', \tag{10}$$

with $N = \int |\phi(0,\tau')|^2\,\mathrm{d}\tau'$ for $z = 10$ mm. Both are in excellent qualitative agreement.

In conclusion, we showed that there exists a limit in the group-velocity mismatch of the constituents of a solitonic two-frequency pulse compound, above which its existence is not possible anymore. We clarified the breakup dynamics for the compound states beyond that limit, and showed that every constituent takes away parts of the radiation, again depending on the relative group velocities. The velocity of the pulse compound before the breakup is determined mostly by its "heaviest" component. More generally, our work demonstrates clearly the limits of stability of multicolor solitonic pulse compounds and we expect that the presented

crossover-phenomenon will be useful for studying and understanding the break-up dynamics of more complex multi-frequency compounds, such as the recently demonstrated polychromatic soliton molecules[43].

Methods

Below we derive a simplified theoretical model, allowing to estimate the parameter range of $\Delta\omega$ that supports formation of two-frequency pulse compounds discussed in the main text. Starting point of our consideration is the first order nonlinear propagation equation for the analytic signal [Eq. (1)], with propagation constant $\beta(\omega)$ and coefficient function $\gamma(\omega)$ given by Eqs. (2) and (3), respectively, together with initial conditions of the form of Eq. (5). We then make the following assumptions and approximation steps:

1. Introducing a reference frequency and shifting to a moving frame of reference[49]. We choose the reference frequency ω_0, for which $\beta(\omega_0) = \beta_0$ and $\beta_1(\omega_0) = \beta_1$, and consider the frequency detuning $\Omega = \omega - \omega_0$ to define the complex envelope

$$\psi(z,\tau) = \sum_{\Omega} \psi_\Omega(z) e^{-i\Omega\tau}, \quad \text{with} \quad \psi_\Omega(z) = \mathcal{E}_{\omega_0+\Omega}(z) e^{-i(\beta_0+\beta_1\Omega)z}, \quad \text{and} \quad \tau = t - \beta_1 z, \tag{11}$$

for which Eq. (1) takes the form

$$i\partial_z\psi_\Omega + [\beta(\omega_0+\Omega) - \beta_0 - \beta_1\Omega]\psi_\Omega + \gamma(\omega_0+\Omega)\left(|\psi|^2\psi\right)_\Omega = 0. \tag{12}$$

The initial condition Eq. (5) then reads

$$\psi(0,\tau) = \left(A_1 e^{-i\Omega_1\tau} + A_2 e^{-i\Omega_2\tau}\right)\mathrm{sech}(\tau/t_0), \tag{13}$$

with $\Omega_{1,2} = \omega_{1,2} - \omega_0$ and $A_{1,2} = \sqrt{|\beta_2(\omega_0+\Omega_{1,2})|/\gamma(\omega_0+\Omega_{1,2})}/t_0$. Let us note that, considering $\beta(\omega_0+\Omega)$ given by Eq. (2), and $\gamma(\omega_0+\Omega) = \gamma_0$, allows to simplify Eq. (12) to the higher-order nonlinear Schrödinger equation

$$i\partial_z\psi_\Omega + \left(\frac{\beta_2}{2}\Omega^2 + \frac{\beta_4}{24}\Omega^4\right)\psi_\Omega + \gamma_0\left(|\psi|^2\psi\right)_\Omega = 0. \tag{14}$$

For parameter values $\beta_2 > 0$ and $\beta_4 < 0$, as we do consider here [see parameters listed right after Eq. (2)], Eq. (14) specifies the frequency domain representation of the model in which generalized dispersion Kerr solitons where demonstrated[42].

2. Approximating the dynamics of a two-pulse initial condition [Eq. (13)], governed by Eq. (12), by a system of coupled higher-order nonlinear Schrödinger equations. Therefore, we define two distinct fields

$$\chi^{(1,2)}(z,\tau) = \sum_{\varpi} \chi^{(1,2)}_\varpi(z) e^{-i\varpi\tau}, \tag{15}$$

taken at the center frequencies $\Omega_{1,2}$ of the two pulses with ϖ denoting the respective frequency detuning, and consider instead of Eq. (12) the pair of coupled equations

$$i\partial_z\chi^{(1)}_\varpi + \left(\beta_0^{(1)} + \beta_1^{(1)}\varpi + \frac{\beta_2^{(1)}}{2}\varpi^2 + \frac{\beta_3^{(1)}}{6}\varpi^3 + \frac{\beta_4^{(1)}}{24}\varpi^4\right)\chi^{(1)}_\varpi + \gamma^{(1)}\left(|\chi^{(1)}|^2\chi^{(1)} + 2|\chi^{(2)}|^2\chi^{(1)}\right)_\varpi = 0, \tag{16}$$

$$i\partial_z\chi^{(2)}_\varpi + \left(\beta_0^{(2)} + \beta_1^{(2)}\varpi + \frac{\beta_2^{(2)}}{2}\varpi^2 + \frac{\beta_3^{(2)}}{6}\varpi^3 + \frac{\beta_4^{(2)}}{24}\varpi^4\right)\chi^{(2)}_\varpi + \gamma^{(2)}\left(|\chi^{(2)}|^2\chi^{(2)} + 2|\chi^{(1)}|^2\chi^{(2)}\right)_\varpi = 0. \tag{17}$$

In the linear parts of Eqs. (16, 17) we introduced the modified dispersion parameters $\beta_n^{(1,2)} \equiv \partial_\Omega^n[\beta(\omega_0+\Omega) - \beta_0 - \beta_1\Omega]_{\Omega=\Omega_{1,2}}$, local to the center frequencies of both pulses. In the nonlinear parts of Eqs. (16, 17) we made the simplifying assumptions $\gamma^{(1,2)} = \gamma(\omega_0+\Omega_{1,2})$ and kept only the effects of self-phase modulation and mutual cross-phase modulation. We might then approximate the dynamics of an initial condition of the form of Eq. (13), evolving under the single equation Eq. (12), by the pair of coupled equations Eqs. (16, 17) with initial conditions

$$\chi^{(1,2)}(0,\tau) = A_{1,2}\mathrm{sech}(\tau/t_0), \quad \text{where} \quad A_{1,2} = \sqrt{|\beta_2^{(1,2)}|/\gamma^{(1,2)}}/t_0. \tag{18}$$

Thereby we further assume the spectral width of either pulse to be small compared to the separation of the pulses center frequencies. Let us note that in the special case where we use Eq. (12) to simulate the dynamics of a single pulse initial condition $\psi(0,\tau) = A_1 e^{-i\Omega_1\tau}\mathrm{sech}(\tau/t_0)$ we can write $\chi^{(1)}(z,\tau) = \sum_\varpi \psi_{\Omega_1+\varpi} e^{-i\varpi\tau} = \psi(z,\tau)e^{i\Omega_1\tau}$, so that $\chi(0,\tau) = A_1\mathrm{sech}(\tau/t_0)$ follows immediately.

3. We make the simplifying assumption that $\beta_n^{(1,2)} = 0$ for $n > 2$ in Eqs. (16, 17) and neglect the cross-phase modulation contribution in Eq. (16). The latter implies that the dynamics of $\chi^{(1)}$, which represents the pulse with larger amplitude, is not affected by $\chi^{(2)}$. Under these assumptions, Eq. (16) with $\chi^{(1)}(0,\tau) = A_1\mathrm{sech}(\tau/t_0)$ constitutes a standard nonlinear Schrödinger equation for a fundamental soliton. We may further use the transformation

$$\phi(z,\tau') = \sum_{\varpi} \phi_{\varpi} e^{-i\varpi\tau'}, \quad \text{with} \quad \phi_{\varpi}(z) = \chi^{(2)}_{\varpi}(z) e^{-i\left(\beta_0^{(2)} + \beta_1^{(1)}\varpi\right)z}, \quad \text{and} \quad \tau' = \tau - \beta_1^{(1)} z, \tag{19}$$

to formally remove the term $\propto \beta_0^{(2)}$ from Eq. (17) and shift to a reference frame in which $|\chi^{(2)}|^2$ is stationary. Abbreviating $\Delta\beta_1 \equiv \beta_1^{(2)} - \beta_1^{(1)}$ and introducing the potential $U(\tau') \equiv -2\gamma^{(2)}|\chi^{(1)}(0,\tau')|^2 = -2\gamma^{(2)} A_1^2 \mathrm{sech}^2(\tau'/t_0)$ we obtain

$$i\partial_z \phi_{\varpi} + \left(\Delta\beta_1 \varpi + \frac{\beta_2^{(2)}}{2}\varpi^2\right)\phi_{\varpi} + \left(\gamma^{(2)}|\phi|^2\phi - U\phi\right)_{\varpi} = 0. \tag{20}$$

We further consider the single soliton initial condition $\phi(0,\tau') = A_2 \mathrm{sech}(\tau'/t_0)$ [cf. Eq. (18)], initially localized at the center of the potential well. Let us note that in Eq. (19) $\tau' = t - \left(\beta_1 + \beta_2\Omega_1 + \frac{\beta_4}{6}\Omega_1^3\right)z = t - \beta_1(\omega_0 + \Omega_1)z$, which verifies that Eq. (20) is in a reference frame in which the potential, representing the pulse at $\omega_1 = \omega_0 + \Omega_1$, is at rest.

The time-domain representation of Eq. (20), given by

$$i\partial_z \phi(z,\tau') + \left[i\Delta\beta_1 \partial_{\tau'} - \frac{\beta_2^{(2)}}{2}\partial_{\tau'}^2 - U(\tau') + \gamma^{(2)}|\phi(z,\tau')|^2\right]\phi(z,\tau') = 0, \tag{21}$$

constitutes the simplified model which allows to estimate the parameter range in which two-frequency pulse compounds are formed (see Discussion in the main text). Let us note that Eq. (21) represents a nonlinear Schrödinger equation with an attractive external potential of sech-squared shape. Similar model equations were previously used to study soliton-defect collisions in the nonlinear Schrödinger equation[59,60], and interaction of matter-wave solitons with quantum wells in the one-dimensional Gross-Pitaevskii equation[61]. While these studies considered the collision of a soliton with an external attractive potential, our aim is here to understand the escape of a soliton from such a potential.

Received: 26 February 2021; Accepted: 13 May 2021
Published online: 27 May 2021

References

1. Drazin, P. G. & Johnson, R. S. *Solitons: An Introduction* (Cambridge University Press, 1989).
2. Kivshar, Y. S. & Agrawal, G. P. *Optical Solitons: From Fibers to Photonic Crystals* (Academic Press, 2003).
3. Mitschke, F. *Fiber Optics: Physics and Technology* (Springer, 2010).
4. Stegeman, G. I. & Segev, M. Optical spatial solitons and their interactions: Universality and diversity. *Science* **286**, 1518–1523 (1999).
5. Akhmediev, N. & Karlsson, M. Cherenkov radiation emitted by solitons in optical fibers. *Phys. Rev. A* **51**, 2602 (1995).
6. Yulin, A. V., Skryabin, D. V. & Russel, P. S. J. Four-wave mixing of linear waves and solitons in fibers with higher-order dispersion. *Opt. Lett.* **29**, 2411 (2004).
7. Tsoy, E. N. & de Sterke, C. M. Theoretical analysis of the self-frequency shift near zero-dispersion points: Soliton spectral tunneling. *Phys. Rev. A* **76**, 043804 (2007).
8. Höök, A. & Karlsson, M. Ultrashort solitons at the minimum-dispersion wavelength: Effects of fourth-order dispersion. *Opt. Commun.* **18**, 1388 (1993).
9. Karlsson, M. & Höök, A. Soliton-like pulses governed by fourth-order dispersion in optical fibers. *Opt. Commun.* **104**, 303 (1994).
10. Piché, M., Cormier, J. F. & Zhu, X. Bright optical soliton in the presence of fourth-order dispersion. *Opt. Lett.* **21**, 845 (1996).
11. Blanco-Redondo, A. *et al.* Pure-quartic solitons. *Nat. Commun.* **7**, 10427 (2016).
12. Kruglov, V. I. & Harvey, J. D. Solitary waves in optical fibers governed by higher-order dispersion. *Phys. Rev. A* **98**, 063811 (2018).
13. Schürmann, H. W. & Serov, V. Comment on "Solitary waves in optical fibers governed by higher-order dispersion". *Phys. Rev. A* **100**, 057801 (2019).
14. Kruglov, V. I. & Harvey, J. D. Reply to "Comment on "Solitary waves in optical fibers governed by higher-order dispersion"". *Phys. Rev. A* **100**, 057802 (2019).
15. Kruglov, V. I. Solitary wave and periodic solutions of nonlinear Schrödinger equation including higher order dispersions. *Opt. Commun.* **472**, 125866 (2020).
16. Kruglov, V. I. & Triki, H. Quartic and dipole solitons in a highly dispersive optical waveguide with self-steepening nonlinearity and varying parameters. *Phys. Rev. A* **102**, 043509 (2020).
17. Stratmann, M., Pagel, T. & Mitschke, F. Experimental observation of temporal soliton molecules. *Phys. Rev. Lett.* **95**, 143902 (2005).
18. Ueda, T. & Kath, W. L. Dynamics of coupled solitons in nonlinear optical fibers. *Phys. Rev. A* **42**, 564 (1990).
19. Afanas'ev, V. V., Dianov, E. M., Prokhorov, A. M. & Serkin, V. N. Nonlinear pairing of light and dark optical solitons. *Pisma Zh. Eksp. Teor. Fiz.* **48**, 588 (1988) **(JETP Lett. 48, 638 (1988))**.
20. Trillo, S., Wabnitz, S., Wright, E. M. & Stegeman, G. I. Optical solitary waves induced by cross-phase modulation. *Opt. Lett.* **13**, 871 (1988).
21. Menyuk, C. R. Stability of solitons in birefringent optical fibers. II. Arbitrary amplitudes. *J. Opt. Soc. Am. B* **5**, 392 (1988).
22. Afanasjev, V. V., Dianov, E. M. & Serkin, V. N. Nonlinear pairing of short bright and dark soliton pulses by phase cross modulation. *IEEE J. Quantum Electron.* **25**, 2656 (1989).
23. Afanasyev, V. V., Kivshar, Yu. S., Konotop, V. V. & Serkin, V. N. Dynamics of coupled dark and bright optical solitons. *Opt. Lett.* **14**, 805 (1989).
24. Menyuk, C. R. Pulse propagation in an elliptically birefingent Kerr medium. *IEEE J. Quantum Electron.* **25**, 2674 (1989).
25. Cao, X. D. & Meyerhofer, D. D. Soliton collisions in optical birefringent fibers. *J. Opt. Soc. Am. B* **11**, 380 (1994).
26. Oreshnikov, I., Driben, R. & Yulin, A. Dispersive radiation and regime switching of oscillating bound solitons in twin-core fibers near zero-dispersion wavelength. *Phys. Rev. A* **96**, 013809 (2017).
27. Krupa, K., Nithyanandan, K., Andral, U., Tchofo-Dinda, P. & Grelu, P. Real-time observation of internal motion within ultrafast dissipative optical soliton molecules. *Phys. Rev. Lett.* **118**, 243901 (2017).

28. Wang, Z. Q., Nithyanandan, K., Coillet, A., Tchofo-Dinda, P. & Grelu, P. Optical soliton molecular complexes in a passively mode-locked fibre laser. *Nat. Commun.* **10**, 830 (2019).
29. Melchert, O. *et al.* Soliton molecules with two frequencies. *Phys. Rev. Lett.* **123**, 243905 (2019).
30. Demircan, A., Amiranashvili, Sh. & Steinmeyer, G. Controlling light by light with an optical event horizon. *Phys. Rev. Lett.* **106**, 163901 (2011).
31. Smith, R. The reflection of short gravity waves on a non-uniform current. *Math. Proc. Cambridge Philos. Soc.* **78**, 517 (1975).
32. de Sterke, C. M. Optical push broom. *Opt. Lett.* **17**, 914 (1992).
33. Philbin, T. G. *et al.* Fiber-optical analog of the event horizon. *Science* **319**, 1367 (2008).
34. Faccio, D. Laser pulse analogues for gravity and analogue Hawking radiation. *Cont. Phys.* **1**, 1 (2012).
35. Plansinis, B. W., Donaldson, W. R. & Agrawal, G. P. What is the temporal analog of reflection and refraction of optical beams?. *Phys. Rev. Lett.* **115**, 183901 (2015).
36. Demircan, A., Amiranashvili, Sh., Brée, C. & Steinmeyer, G. Compressible octave spanning supercontinuum generation by two-pulse collisions. *Phys. Rev. Lett.* **110**, 233901 (2013).
37. Demircan, A., Amiranashvili, Sh., Brée, C., Morgner, U. & Steinmeyer, G. Adjustable pulse compression scheme for generation of few-cycle pulses in the midinfrared. *Opt. Lett.* **39**, 2735 (2014).
38. Driben, R., Mitschke, F. & Zhavoronkov, N. Cascaded interactions between Raman induced solitons and dispersive waves in photonic crystal fibers at the advanced stage of supercontinuum generation. *Opt. Express* **18**, 25993 (2010).
39. Demircan, A. *et al.* Rogue events in the group velocity horizon. *Sci. Rep.* **2**, 850 (2012).
40. Demircan, A. *et al.* Rogue wave formation by accelerated solitons at an optical event horizon. *Appl. Phys. B* **115**, 343 (2014).
41. Armaroli, A., Conti, C. & Biancalana, F. Rogue solitons in optical fibers: A dynamical process in a complex energy landscape?. *Optica* **2**, 497 (2015).
42. Tam, K. K. K., Alexander, T. J., Blanco-Redondo, A. & de Sterke, C. M. Generalized dispersion Kerr solitons. *Phys. Rev. A* **101**, 043822 (2020).
43. Lourdesamy, J. P., Runge, A. F. J., Alexander, T. J., Hudson, D. D., Blanco-Redondo, A. & de Sterke, C. M. Polychromatic soliton molecules. Preprint at https://arxiv.org/abs/2007.01351 (2020).
44. Hu, G. *et al.* Asynchronous and synchronous dual-wavelength pulse generation in a passively mode-locked fiber laser with a mode-locker. *Opt. Lett.* **42**, 4942 (2017).
45. Zhang, X. *et al.* Design of a dual-channel modelocked fiber laser that avoids multi-pulsing. *Opt. Exp.* **27**, 14173 (2019).
46. Moille, G., Li, Q., Kim, S., Westly, D. & Srinivasan, K. Phased-locked two-color single soliton microcombs in dispersion-engineered Si_3N_4 resonators. *Opt. Lett.* **43**, 2772 (2018).
47. Melchert, O., Yulin, A. & Demircan, A. Dynamics of localized dissipative structures in a generalized Lugiato-Lefever model with negative quartic group-velocity dispersion. *Opt. Lett.* **45**, 2764 (2020).
48. Weng, W., Bouchand, R. & Kippenberg, T. J. Formation and collision of multistability-enabled composite dissipative Kerr solitons. *Phys. Rev. X* **10**, 021017 (2020).
49. Amiranashvili, Sh. & Demircan, A. Hamiltonian structure of propagation equations for ultrashort optical pulses. *Phys. Rev. A* **82**, 013812 (2010).
50. Amiranashvili, Sh. & Demircan, A. Ultrashort optical pulse propagation in terms of analytic signal. *Adv. Opt. Technol.* **2011**, 989515 (2011).
51. Melchert, O., Roth, B., Morgner, U. & Demircan, A. OptFROG—Analytic signal spectrograms with optimized time-frequency resolution. *SoftwareX* **10**, 100275 (2019).
52. Melchert, O., Morgner, U.Roth, B., Babushkin, I. & Demircan, A. Accurate propagation of ultrashort pulses in nonlinear waveguides using propagation models for the analytic signal. In *Computational Optics II* (eds. Smith, D. G. *et al.*) 103–113 (SPIE, 2018).
53. Haus, H. A. & Ippen, E. P. Group velocity of solitons. *Opt. Lett.* **26**, 1654 (2001).
54. Pickartz, S., Bandelow, U. & Amiranashvili, Sh. Adiabatic theory of solitons fed by dispersive waves. *Phys. Rev. A* **94**, 033811 (2016).
55. Saleh, M. F. & Biancalana, F. Soliton-radiation trapping in gas-filled photonic crystal fibers. *Phys. Rev. A* **87**, 043807 (2013).
56. Afanasjev, V. V. & Vysloukh, V. A. Interaction of initially overlapping solitons with different frequencies. *J. Opt. Soc. Am. B* **11**, 2385 (1994).
57. Feigenbaum, E. & Orenstein, M. Coherent interactions of colored solitons via parametric processes: Modified perturbation analysis. *J. Opt. Soc. Am. B* **22**, 1414 (2005).
58. Kodama, J. & Hasegawa, A. Effects of initial overlap on the propagation dynamics of optical solitons at different wavelengths. *Opt. Lett.* **16**, 208 (1991).
59. Cao, X. D. & Malomed, B. A. Soliton-defect collisions in the nonlinear Schrödinger equation. *Phys. Lett. A* **206**, 177 (1995).
60. Goodman, R. H., Holmes, P. J. & Weinstein, M. I. Strong NLS soliton-defect interactions. *Phys. D* **192**, 215 (2004).
61. Ernst, T. & Brand, J. Resonant trapping in the transport of a matter-wave soliton through a quantum well. *Phys. Rev. A* **81**, 033614 (2010).

Acknowledgements

The authors acknowledge financial support from the Deutsche Forschungsgemeinschaft (DFG) under Germany's Excellence Strategy within the Clusters of Excellence PhoenixD (Photonics, Optics, and Engineering – Innovation Across Disciplines) (EXC 2122, projectID 390833453) and QuantumFrontiers (EXC 2123, projectId 390837967).

Author contributions

O.M. performed the numerical simulations and analysis. S.W. supported the numerical simulations. O.M., S.W., U.M., I.B. and A.D. interpreted the results and contributed to the manuscript. A.D. headed the project throughout.

Funding

Open Access funding enabled and organized by Projekt DEAL.

Competing interests

The authors declare no competing interests.

Additional information

Correspondence and requests for materials should be addressed to O.M.

Reprints and permissions information is available at www.nature.com/reprints.